Precision Engineering 36 (2012) 485–493

Contents lists available at SciVerse ScienceDirect

Precision Engineering

journal homepage: www.elsevier.com/locate/precision

A BPNN-PID based long-stroke nanopositioning control scheme driven by ultrasonic motor

Fang Cheng[a,c,1,3], Kuang-Chao Fan[a,b,*,2], Jinwei Miao[a,1], Bai-Kun Li[b,2], Hung-Yu Wang[b,2]

[a] School of Instrument Science and Opto-electronics Engineering, Hefei University of Technology, Anhui, 230009, China
[b] Department of Mechanical Engineering, National Taiwan University, Taipei, Taiwan
[c] School of Mechanical & Aerospace Engineering, Nanyang Technological University, Singapore

ARTICLE INFO

Article history:
Received 3 October 2011
Received in revised form 23 February 2012
Accepted 6 March 2012
Available online 17 March 2012

Keywords:
Nanopositioning
Ultrasonic motor
LDGI
Robust control
Repeatability

ABSTRACT

In this paper an innovative nanopositioning control scheme for different travel lengths is proposed. A commercial ultrasonic motor HR4 and its driver AB2 are employed to generate 3-mode motions (AC, Gate, and DC modes) to accommodate different travels, speeds and resolutions. For precise displacement feedback, a new displacement sensor LDGI (linear diffraction grating interferometer) is developed to meet the requirements of both long range and nano resolution. A key technology in this study is the proposed positioning control algorithm for the linear stage driven by HR4 and AB2. A 3-mode digital PID controller with a self-tuning module by back propagation neural network (BPNN) is developed for multi-scale and all-in-one motion control of 3 modes. Both experiments and software simulation show that this software-based controller developed by LabVIEW has good capability to overcome the uneven friction of the sliding plane and to lock the final position stably. The highlight of this 3-step motion control system is first to drive the table by AC mode at a low and stable speed in millimeter per second scale, then to move close to the target point by Gate mode with the positioning error less than 100 nm in micrometer per second scaled speed, and finally to adjust and hold at the target point by DC mode in nanometer per second scaled speed. In the experiments of different travels up to 15 mm, calibrated by a commercial laser interferometer, the positioning accuracy is proved within 10 nm with standard deviation less than 5 nm and the final position locking can be limited to 3 nm.

1. Introduction

A general close-loop positioning system needs at least three components: actuator, displacement feedback and control scheme. For a positioning system with a scale-to-tolerance ratio larger than 10^6, a driving system with acceptable performance in both macroscale and nanoscale is needed [1]. A conventional leadscrew–rotary motor system is usually difficult to meet the requirement of high precision positioning accuracy in long stroke, because of some inherent problems, such as backlash, inadequate resolution, and stick-slip [2–4]. Piezoelectric actuators are widely used in nanopositioning for its high resolution, but their travel ranges are limited to several tens of micrometers only. An inchworm-type linear piezomotor can provide a travel range of several millimeters, but the output force is very small. Besides, a behavior called "glitching" is resulted from the piezomotor design [5]. In [6] an inchworm type driving system is developed with piezoelectric elements to realize nanopositioning over millimeter-scaled traveling length, but only to 5 mm and the resolution cannot be higher than 5 nm. Chu [7] developed a long travel piezoelectric-driven linear positioning stage using the principle of a stick–slip linear micropositioner, but the longest travel was only up to 50 μm and no control scheme was employed. Another design of long-stroke positioning is a stacked up type two-stage table comprising a servo motor stage for long-stroke and a PZT stage for fine motion [8–11]. Liu et al. [12] adopted traditional PID controller for both coarse (ball-screw) and fine (PZT) stages. Kawashima et al. [13] adopted propositional controller for coarse stage (air cylinder) and PI control for fine stage (voice coil motor, VCM). Liu [14] applied PI controller for coarse motion (VCM) and P controller for fine motion (PZT). The mechanical structure and the control loop of this two-stage type are, however, too complicated. Using a single stage to achieve both long-stroke and fine motions with a proper controller is deemed simpler in structure.

The design and control of a single stage for long-stroke nanopositioning control has received a great attention in recent years due to the demands of fabricating or measuring micro structures

* Corresponding author at: Department of Mechanical Engineering, National Taiwan University, Taipei, Taiwan. Tel.: +886 2 2362 0032.
E-mail address: fan@ntu.edu.tw (K.-C. Fan).
[1] Tel.: +86 551 2903823.
[2] Tel.: +886 2 2362 0032.
[3] Tel.: +65 6790 5576.

0141-6359/$ – see front matter © 2012 Elsevier Inc. All rights reserved.
doi:10.1016/j.precisioneng.2012.03.001

on a large surface in the fields of lithography, micromachining, display technology, and micro/nano-CMM. Making use an ultrasonic motor to dive a single stage in friction mode for both the long-stroke and nanopositioning motion control is one of the selections. Egashira et al. [15–17] developed a nonresonant ultrasonic motor (NRUSM) to drive a lithography precision stage fed back by a Sony BS76 linear scale (resolution to 10 nm). The 300 mm stroke was driven by AC mode at fast feed velocity to 85 mm/s only with open-loop control and the short stroke up to was carried out by DC mode with PID control to the best positioning accuracy of ±0.69 nm (measured by HP5529A laser interferometer), being a remarkable achievement. Since the applied lithography stage required fast velocity in long-stroke motion, the friction effect, which is sensitive to low speed motion, was not considered in their AC mode.

The ultrasonic motor has the advantages of compact structure and the capability of integrating multi-scale driving modes in an all-in-one actuator. Its motion control scheme, however, still remains challenging task because it typically uses the side friction as the driving force without a speed reduction mechanism, which means the stability will be very sensitive to the friction change along the guide way, especially for low-speed and long-stroke control. Conventional PID controller with fixed parameters cannot overcome the problem when the uneven surface friction generated velocity variation is large. Some adaptive PID controllers were thus used. For example, Tanaka adopted neural network (NN)-PID controller to overcome the time-variant characteristics of the ultrasonic motor for precision motion control [18]; Zhao used back propagation (BP) fuzzy NN to control ultrasonic motor's velocity, but only gave simulation results [19]; Senjyu [20] investigated the speed control of ultrasonic motor using BPNN algorithm but no practical applications; and Lin [21] applied recurrent fuzzy NN control for ultrasonic motor drive.

The author's group has previously developed a FCMAC controller on a self-designed co-planar stage driven by the commercial ultrasonic motor (HR4) and its driver (AB2) for more stable velocity during motion in AC mode [22]. However, the signal fluctuation on the feedback sensor of a linear diffraction grating interferometer (LDGI) caused by the excited frequency of HR4 still affected the controller. It did not show the results of long-stroke positioning accuracy, only the short-stroke control of discrete steps by GATE and DC modes were given. In another report, the author's group has preliminarily studied the performance of an ultrasonic motor in different scales and proposed a neural network motion controller for both speed control in coarse motion and position control in fine motion on a commercial stage [23], but how to hold the final position was unsolved.

In this report, an improved BPNN-PID controller is proposed for the long-stroke and nanopositioning control of a new co-planar linear stage driven by HR4 and AB2. Compared with our previous system [22,23], the feedback sensor of LDGI has been modified to allow easier assembly and the co-planar stage is also modified to eliminate the high frequency disturbance on the LDGI caused by the exciting force of HR4. This is a software-based controller developed around the LabVIEW environment in a PC. As the stage is used for a micro-CMM [24], the long-stroke motion is at low speed of 1 mm/s driven by AC mode with BPNN-PID for stable velocity to overcome the friction changes due to uneven surface morphology of the sliding plane, the short step motion is actuated by GATE mode with position feedback control, and the fine motion is driven by DC mode with BPNN-PID for final position locking and anti-disturbance. In the experiments of different travels up to 15 mm, calibrated by a commercial laser interferometer, the positioning accuracy is proved within 10 nm with standard deviation less than 5 nm and the final position locking can be limited to 3 nm.

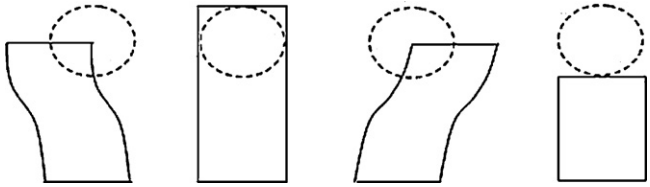

Fig. 1. The elliptical motion of piezoelectric elements.

2. Integration of three driving modes

2.1. The principle of ultrasonic motor HR4

The ultrasonic motor HR4 has four piezoelectric elements [25]. When the voltage is applied across these elements at a resonate frequency of 39.6 KHz, the front edge of the motor generates an elliptical motion, which is the vector sum of the bending mode and the longitudinal mode, as shown in Fig. 1. This elliptical motion then drives the stage through a contact tip by friction force to create linear motion of the stage.

2.2. Three driving modes of AB2

The HR4 is actuated by the AB2 driver developed by the Nanomotion Co. [25]. The AB2 drive box consists of a single card (command source) that converts the input command signal into a corresponding PWM output signal. In this mode the output transformer–amplifier circuit converts the PWM output signal into a high voltage sine wave that drives the motor. The PWM controller is power-fed from an internal DC-to-DC converter that is fed from an external +24 V power supply. Fig. 2 illustrates a typical application of the AB2 Driver Box.

In this study, the HR4 is associated with AB2 to generate 3-mode motions of different scales.

In AC mode, the HR4 generates a successive motion in the stroke length from 0.1 to 20 mm. The stage is required to control at a low and stable speed of about 1 mm/s. In practice, non-constant friction force between the moving table and the guide way will, however, introduce notable accelerations that will cause unsteady-state motion resulting in positioning errors. Although the positioning error of AC mode can be measured and compensated in GATE and DC modes, to improve the control efficiency, it is necessary to reduce the positioning error in AC mode because the movement in GATE mode is very slow. In this mode the speed is calculated at every millisecond for real-time speed control.

As mentioned in Section 2.1, the friction force of HR4 is directly applied on the stage, without speed reducing mechanism like a ball screw, so the motion is very sensitive to disturbances. Besides, although the successive motion is composed by fine steps of the piezoelectric elements, the steps may have random lengths. Considering HR4 as a black box, a software-based controller is developed to maintain the speed constant. Details will be described in Section 4. After the AC-mode, the moving table is close to the target point within 5 μm.

Then in GATE mode, HR4 drives the table to move in short steps with random increments of 20–50 nm and the total stroke length is within several microns. A suitable close-loop control scheme is also required to move the table until the position to the target is within 30 nm.

Lastly in DC-mode, the HR4 works like a conventional PZT actuator to adjust the position in several nanometers and finally to lock at the target position. For a conventional PZT actuator, a characteristic curve is often used to describe the relationship between the displacement and the driving voltage. It is based on one hypothesis that the friction is constant at every position, which is not

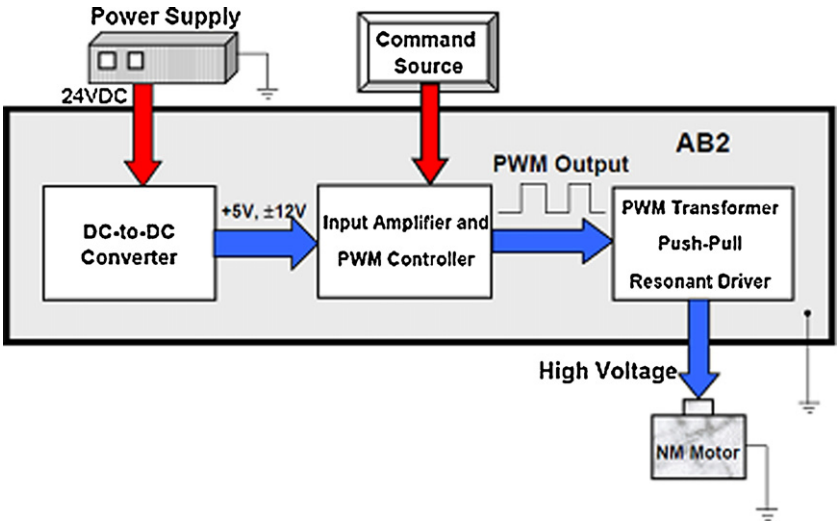

Fig. 2. The AB2 block diagram.

possible due to uneven surface finish conditions of the guide way. A close-loop control scheme is thus necessary in DC mode. It is to compensate for the positioning error after the GATE mode. The position of the table, however, cannot be held by static force because the piezoelectric elements of HR4 and other mechanical elements will release the stress. Besides, some unpredictable disturbances may affect the position. The position adjustment in DC mode will, therefore, be actuated until an external command stops the positioning control.

The above mentioned control processes are illustrated in Fig. 3. The details of different-mode controls will be described in following sections.

3. The displacement sensor LDGI

The position feedback sensor equipped in ordinary precision stages is the linear scale, which normally provides the resolution to 1 or 0.1 μm. Although some commercial linear scales provide nanometer resolution, but all are with accuracy in micron or submicron levels only. This is not adequate enough for nanopositioners. Laser interferometer is the current solution for most ultra precision stages. It is known that laser interferometer is sensitive to the variation of ambient conditions as its basic scale, the wavelength, is temperature-dependent. In addition, the laser interferometer is expensive and its size is normally large in comparison with the size of all fine motion stages. The holographic grating scale measures the displacement of the stage based on its scale pitch, which is immune to atmosphere variations. Although the grid has manufacturing imperfections, but they are generally predictable and can be

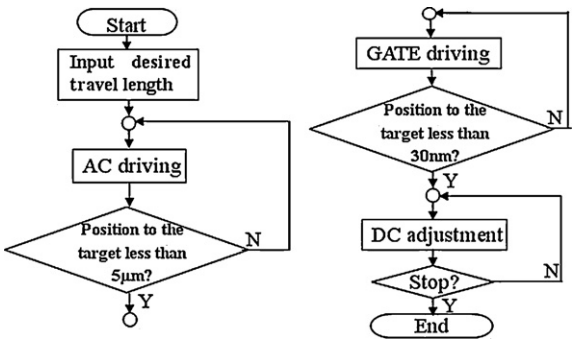

Fig. 3. The flow chart of 3-mode positioning control.

software compensated. Moreover, the grating scale system is very low cost. This is why this system is adopted in this study.

3.1. The principle of LDGI

The structure of the new LDGI is designed in Littrow configuration, as shown in Fig. 4a. Compared to our earlier design of Fig. 4b [22], although the optical principle is similar but the separation of two beams at a required distance has been replaced by a rhomboid prism (RHP) and a right angle prism (RAP). The total number of optical components can be reduced from 14 to 11 (except grating, laser diode, and PDs). The main reason is that the physical dimension of LDGI must be as small as possible in order to mount onto the integrated co-planar stage, which will be shown in Sections 5 and 6. Each optical component is selected the smallest size of 5 mm side length from the market. Bonding optics together into a compact module is an extremely difficult task, not only each one is difficult to be grasped by the hand but also the gluing process will cause a small gap between contact surfaces. Experiments show that the "ghost spots" caused by the redundant reflection between the contacting surfaces obviously influence the signal quality. Moreover, because the redundant reflected beams will also interfere with the normal diffracted beams.

As shown in Fig. 3a, the two diffraction beams are combined at PBS1 and converted into left and right circularly polarized beams by Q3. With the phase shift module composed by NPBS, PBS2 and PBS3, the interference fringe with 90° phase shift can be detected by photodetectors PD1 to PD4. Because of the Doppler shift caused by the grating's lateral motion, the diffraction beams will have a phase shift proportional to the motion speed of the grating. When the grating moves half pitch ($d/2$), the beat frequency signal has a phase variation of one period (360°). With a holographic grating of 1200 lines/mm, there is a wave cycle of the orthogonal signals at every 416 nm of the grating movement.

3.2. Normalization of LDGI signals

Theoretically speaking, LDGI signals are sine and cosine waves with the phase shift of 90°, but the geometrical errors of the mechanical system will cause some signal distortions. There are three fundamental distortions: (1) DC drift, due to the variation of background light on the photo detectors, (2) amplitude variation, due to the angular motions of the linear stage, (3) phase error, due to the installation of optical components. Suppose that the

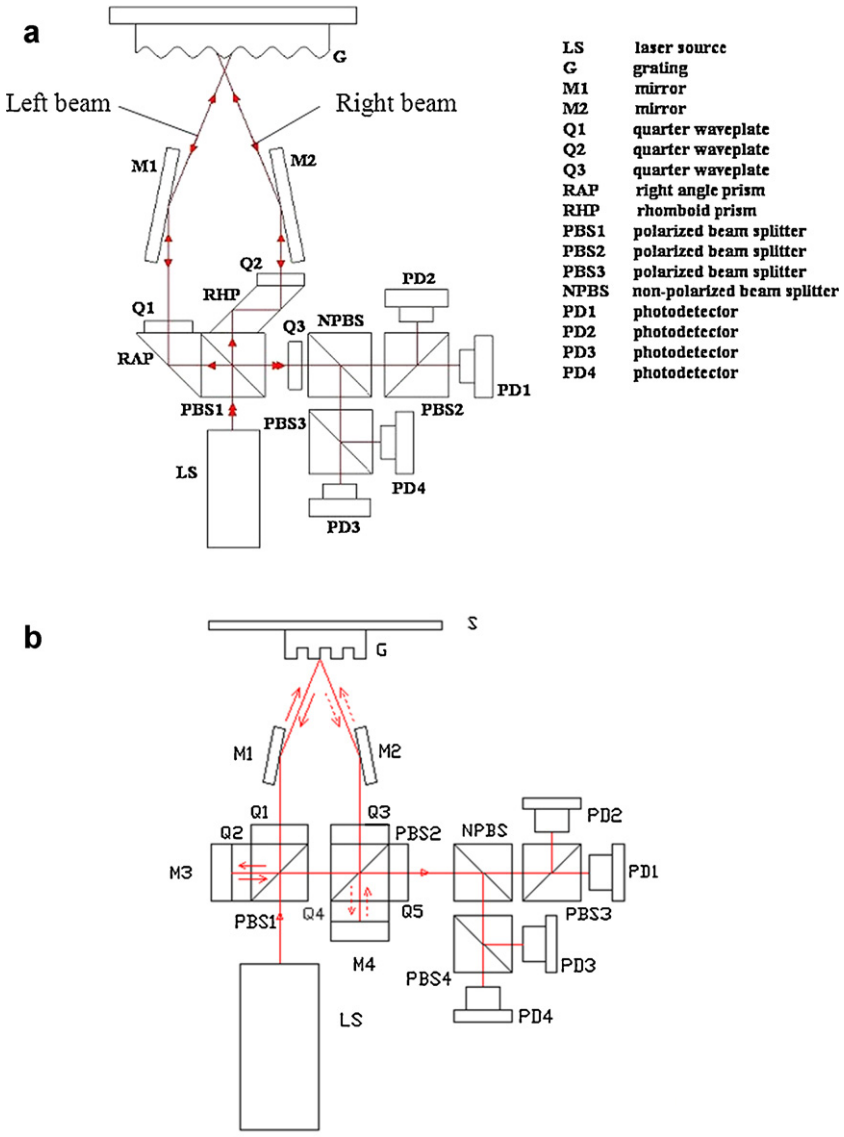

Fig. 4. The optical structure of LDGIs.

original LDGI signals are $f(x)$ and $g(x)$. In every millisecond 1000 data points are sampled and the maximum and minimum values are calculated. Then the envelope curve of the four output waveforms $u(x)$, $u'(x)$ and $v(x)$, $v'(x)$ can be worked out with piecewise linear interpolation [23], as shown in Fig. 5. New waves $f_1(x)$ and $g_1(x)$, without DC drift and amplitude variation are obtained as:

$$f_1(x) = \frac{f(x) - [u(x) + u'(x)]/2}{[u(x) - u'(x)]/2} \tag{1}$$

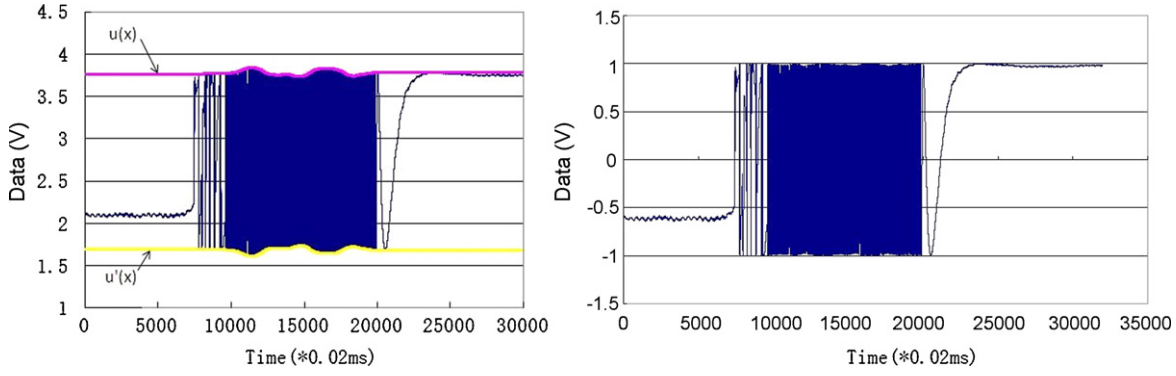

Fig. 5. Signal processing on DC drift and amplitude variation: original signal (left) and processed signal (right). For convenience, only one channel of signal is shown.

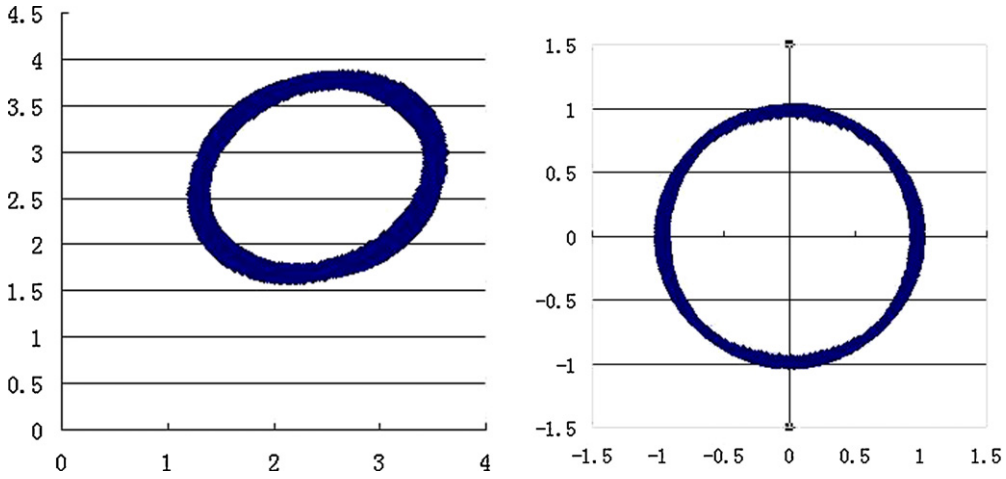

Fig. 6. The Lissjous figure of the LDGI signals before (left) and after (right) the process.

$$g_1(x) = \frac{g(x) - [v(x) + v'(x)]/2}{[v(x) - v'(x)]/2} \tag{2}$$

After DC drift and amplitude variation are eliminated, the phase error is corrected by vector summation and subtraction operations: suppose the two non-orthogonal waveforms are $X = f_1(x) = \sin(x)$ and, $Y = g_1(x) = \sin(x + \varphi)$, where $\varphi \neq 0$, the outputs can be corrected to:

$$f_2(x) = f_1(x) + g_1(x) = \sin(x) + \sin(x + \varphi) = 2 \sin\frac{2x + \varphi}{2} \cos\frac{\varphi}{2} \tag{3}$$

$$g_2(x) = f_1(x) - g_1(x) = \sin(x) - \sin(x + \varphi) = 2 \cos\frac{2x + \varphi}{2} \sin\frac{\varphi}{2} \tag{4}$$

The Lissajous figures of the original signals and the processed signals are shown in Fig. 6.

With pulse count and phase subdivision operations the displacement can be calculated. In every millisecond, the 1000 points of the signal can also be used for real-time speed calculation.

4. Self-tuning PID control algorithm

4.1. Conventional PID control

Conventional PID controller needs constant gains K_p, K_i and K_d, which should be determined from experiments. When the situation such as the friction changes, the parameters K_p, K_i and K_d should be trained again. In this study, a software-based controller has been developed in the LabVIEW environment. Simulations can be carried out to show the performances of various given conditions.

Take AC-mode speed control for instance, the friction and the PID control system can be simulated by the flow chart in Fig. 7. The parameters are defined as follow:

V_j: velocity, the absolute value of the speed, ΔV: the increment of the speed, $U_f(x)$: friction induced driving voltage function, where x means position, U_0: the minimum driving voltage to overcome the friction, δ: a constant to describe the increment of driving voltage at start-up. The maximum static friction, when the speed is 0, is larger than the dynamic friction while moving. This friction difference, which will obviously influence the control performance, will cause the driving voltage difference δ, U_j: the actual driving voltage, ΔU: the increment of driving voltage during motion.

Suppose T is the constant interval of the speed sampling, the acceleration is:

$$a = \frac{\Delta V}{T} \tag{5}$$

The driving force is proportional to the driving voltage $(U_j - U_0)$, which can be expressed as:

$$F = c(U_j - U_0) \tag{6}$$

where c is a constant of the transform coefficient between the voltage and force.

From (5) and (6), when $U_j > U_0$, with the classic Newton Second Law $F = ma$, the following equation can be derived:

$$\Delta V = (U_j - U_0)\frac{cT}{m} \tag{7}$$

For convenience, a constant K is defined as: $K = cT/m$, then $\Delta V = K(U_j - U_0)$, as defined in Fig. 7. Simulation result of an

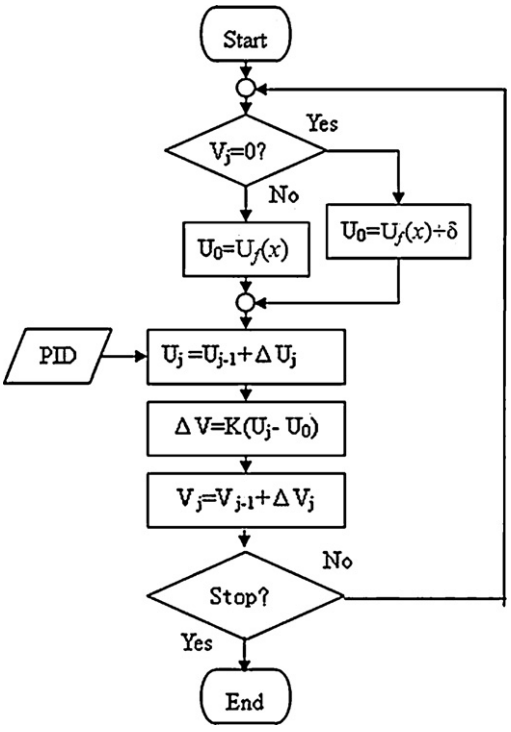

Fig. 7. Flow chart of convention PID speed control.

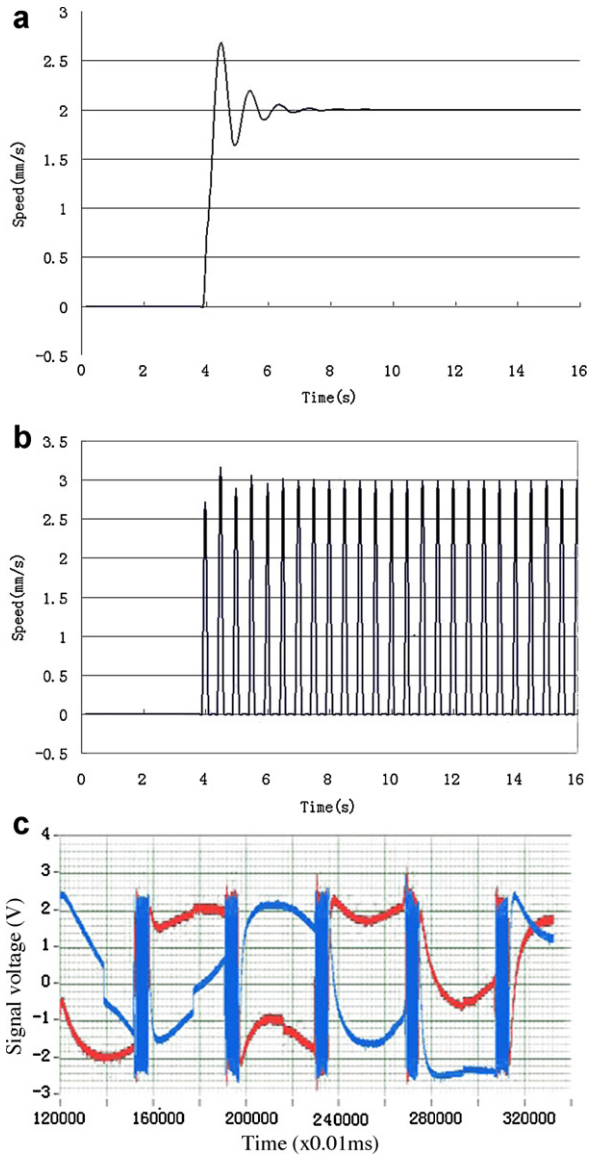

Fig. 8. Performance of conventional PID control.

optimized combination of K_p, K_i and K_d has an acceptable performance if the friction is constant, as shown in Fig. 8a. The same set of K_p, K_i and K_d, however, cannot converge when the friction induced driving voltage function $U_f(x)$ has a notable change, as shown in Fig. 8b. It was found from experiments that when the driving voltage rose continuously from 0 V, the stage would not start moving until the driving voltage reaches 4 V. Once the stage was moved, however, the driving voltage to maintain the stable movement should be reduced to around 1.5 V, otherwise the stage would have a large acceleration which could seriously affect the stability of the mechanic system. This phenomenon obviously shows the influence of sudden friction change, which is expressed by δ in Fig. 7.

For the driving system equipped with ultrasonic motor, the driving force is directly added to the stage without any speed reduction structure. So the system is very sensitive to the friction change in low speed control. The simulation result in Fig. 8b shows the speed curve of the typical discontinuous motion, called low-speed creeping.

In actual driving tests, the LDGI signals are sampled by the DAQ board simultaneously to show the controlling performance. When only the conventional PID controller is employed, this problem can easily be reflected by the discontinuous LDGI signal, as shown in Fig. 8c. A self-tuning module BPNN is therefore introduced to adjust the value of K_p, K_i and K_d in real time.

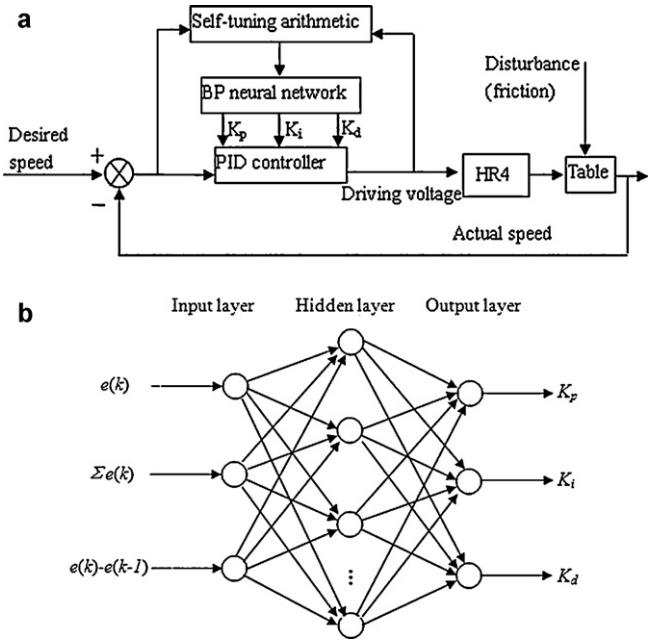

Fig. 9. The theoretical structure of BPNN-based PID control loop.

4.2. BPNN-based PID control loop

For convenience, the principle of the control scheme is mainly illustrated with the speed control in AC mode. The control loop of BPNN-based PID control is shown in Fig. 9. The detailed structure of BPNN is denoted in [26–28].

The principle of the BPNN-based PID control loop can be summarized as below:

Classical PID control algorithm can be described as:

$$u(k) = u(k-1) + K_p[e(k) - e(k-1)] + K_i e(k) + K_d[e(k) - 2e(k-1) + e(k-2)] \quad (8)$$

Among it error $e(k) = r(k) - y(k)$ is the difference of given value and output value in every instant.

There BP neural network, serving as the self-tuning module of K_p, K_i and K_d, is composed by input layer, hidden layer, and output layer. Assuming x_i and y_i are the input and output values of a neural cell, the activation process in this neural cell describes a non-linear relationship, typically expressed by the Sigmoid function [29,30]:

$$y_i = \begin{cases} \tanh(x_i) & \text{in hidden layer} \\ \frac{1}{2}[1 + \tanh(x_i)] & \text{in output layer} \end{cases} \quad (9)$$

The input values of input layer are $e(k)$, $\Sigma e(k)$, and $e(k) - e(k-1)$. For each neural cell of hidden layer and output layer, the input value depends on the output values of front layer cells and the connection weights in between, as shown in Fig. 9b. For example, assuming y_i is the output of the ith cell of a certain layer, and $\omega_{i,j}$ is the connection weight, the input of the jth cell in the next layer can be expressed by:

$$X_j = \sum_{i=1}^{n} \omega_{i,j} y_i \quad (10)$$

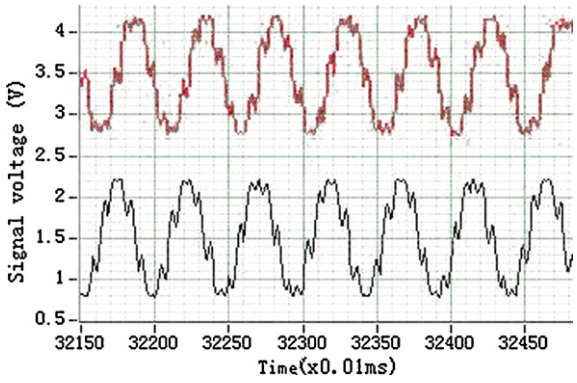

Fig. 10. Harmonic disturbance of LDGI signals caused by HR4.

In order to derive the error back-propagation process, the error energy function is defined as:

$$J = \frac{1}{2}[r(k+1) - y(k+1)]^2 \tag{11}$$

This function, clearly describing the difference between desired output $r(k+1)$ and actual output $y(k+1)$, can be used as the performance function. The connection weight can be adjusted by J in the negative gradient direction (steepest descent method).

In the proposed positioning system, the BPNN-PID controller is used in AC mode for speed control, where the speed is used as the controlled parameter; and in DC mode for position locking, where the displacement is used as the controlled parameter. In GATE mode the stepping stroke is short at very low speed, only a simple close-loop proportional control is used to limit the step length to make sure the last step is within the adjustable range of DC mode.

5. Experimental setup

The developed BPNN-PID controller was integrated into a co-planar linear stage, which provides the X and Y motions of a developed Micro-CMM [24]. In our previous design of the co-planar stage [22], the sensor LDGI and the motor HR4 were mounted on the same side. The inherent vibration signals at 39.6 KHz generated by HR4 will inevitably superimpose on the sinusoidal signals of LDGI, as shown in Fig. 10. Such a higher order harmonic disturbance will by all means yield to wrong pulse counting and phase subdivision processes of LDGI signals. It is why the FCMAC controller employed to the previous stage could only demonstrate the constant speed control for long stroke motion by AC mode and very short positioning control to maximum 10 μm only by GATE and DC modes, individually.

In this study, an improved positioning system is designed as schematically shown in Fig. 11. The central table is moved by an active linear guide in a push–pull mode, which is actuated by the ultrasonic motor HR4 through a friction force on the ceramic plate. The LDGI is moved to the other side of the table and mounted on the passive linear guide whose displacement is synchronized to the table. The harmonic excitation caused by HR4 can thus be entirely removed from the LDGI signals. Since the displacement sensor is in line with the moving axis, it observes the law of Abbé Principle [31].

The LDGI signals are amplified by a processing circuit and sampled by an NI-DAQ card (model PCI-6259). After software processing the current displacement and speed can be calculated and then the optimized driving voltage can be determined by the software-based controller and sent to the driver AB2 through PCI-6259. Calibration of LDGI is carried out with a laser interferometer

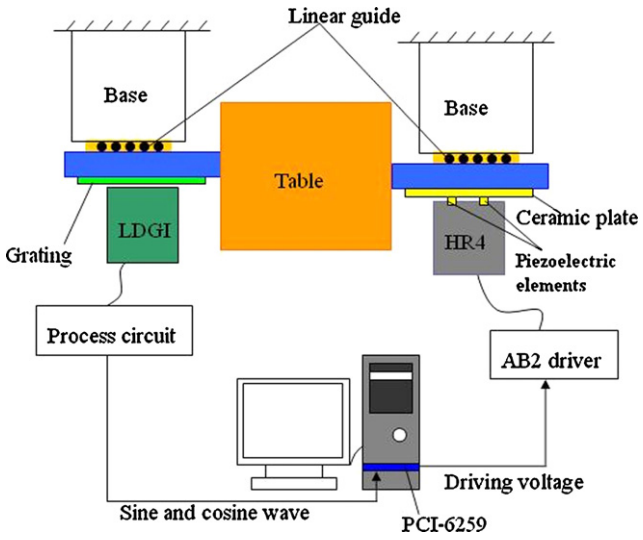

Fig. 11. Configuration of the improved positioning control system.

(MI-5000 of SIOS Co.), whose readings are included in the DLL file and output to the PC through the USB interface.

6. Positioning experiments

To testify the above control scheme, two parts of experiments are designed.

Firstly, assuming that the precision of LDGI is credible, the performance of speed control in AC mode and positioning control in DC mode can be testified as follows:

In AC mode, the desired speed is 1 mm/s. The performance of speed control by BPNN-based PID is shown in Fig. 12. The speed curve seems to be not smooth enough because in every "while loop" during the movement, the time interval to calculate current speed is very short so that speed variation is inevitable. However, because the LDGI is in Littrow configuration and its waveform errors are corrected after normalization, this kind of speed variation will not affect the precise reading of LDGI.

As illustrated in Sections 2.2 and 4.2, GATE mode is just the transition between macroscale and nanoscale control. Since this mode only provides stepwise motions, a normal close-loop control is adequate.

In DC mode, the performance of displacement control with BPNN-based PID is shown in Fig. 13. Fig. 13a shows that the system is able to converge in 2 s. Fig. 13b shows the system can lock the position for a long time with the shift less than 3 nm. Fig. 13c shows when an unpredictable disturbance occurs, such as a knock on table,

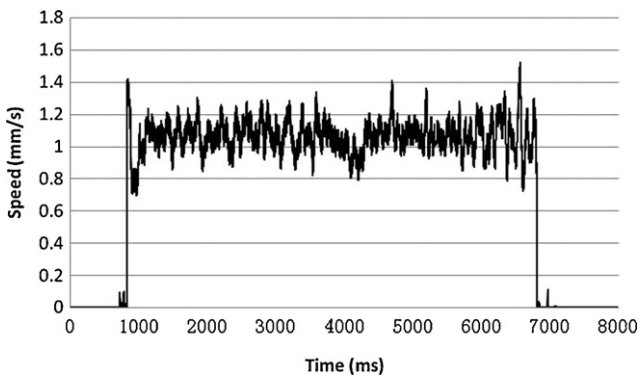

Fig. 12. The controlled speed in AC mode.

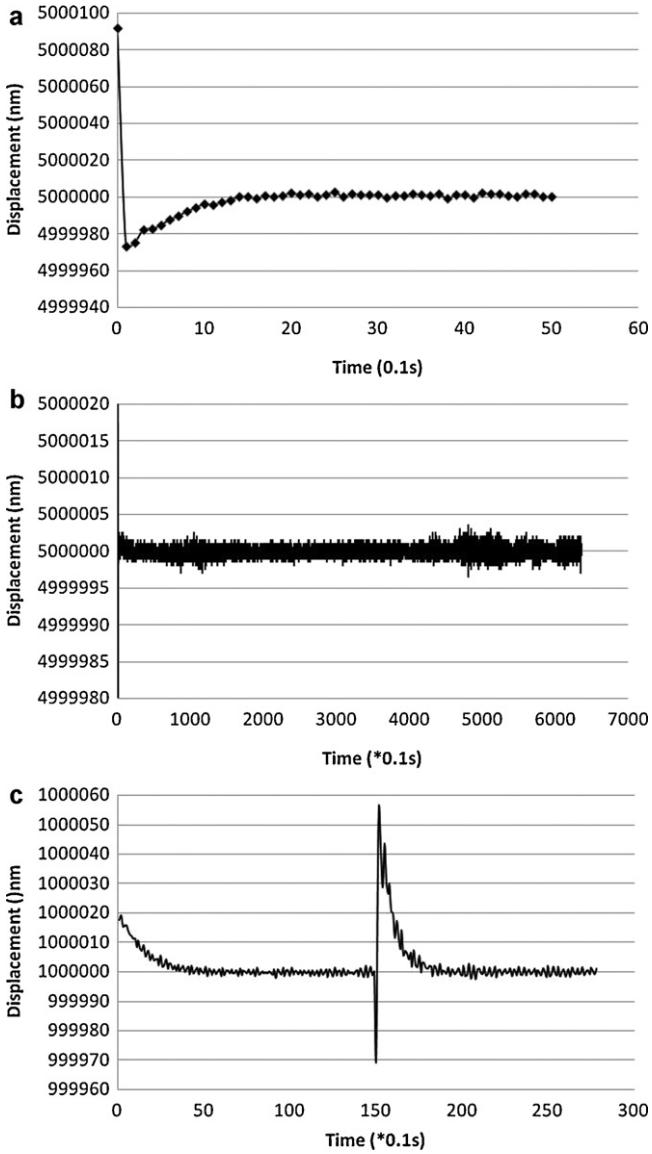

Fig. 13. The control performance in DC mode.

the control system can recover to a new steady state in 2 s.Secondly, to prove the precision of LDGI, a miniature laser interferometer (SIOS Co., model SP-120) is employed as the displacement calibrator. The readings of the laser interferometer and LDGI are sampled simultaneously. The whole system is put in a constant temperature chamber, as shown in Fig. 14. During experiments the temperature variation is between 25.2 °C and 25.3 °C, and the vibration and airflow are isolated effectively. In this environment the LDGI and the SIOS interferometer can have stable readings.

In the primary experiment the data of positioning errors were calibrated at every 1 mm to the total travel of 15 mm and then fitted by a polynomial curve of the 3rd order, as shown in Fig. 15a. Figs. 15(b and c) shows that this polynomial error curve can be separated into two parts: the fundamental linear part due to alignment error in micron scale and the high-order part due to the nonlinearity of the guide way in nanometer scale. Both types of errors can be compensated if the repeatability is good.

Then, five different travel lengths of 0.1 mm, 1 mm, 5 mm, 10 mm, and 15 mm were carried out with the assistance of the error compensation scheme. For each travel length the positioning experiment is repeated 5 times and the compensated errors are listed in Table 1. It is demonstrated that the proposed

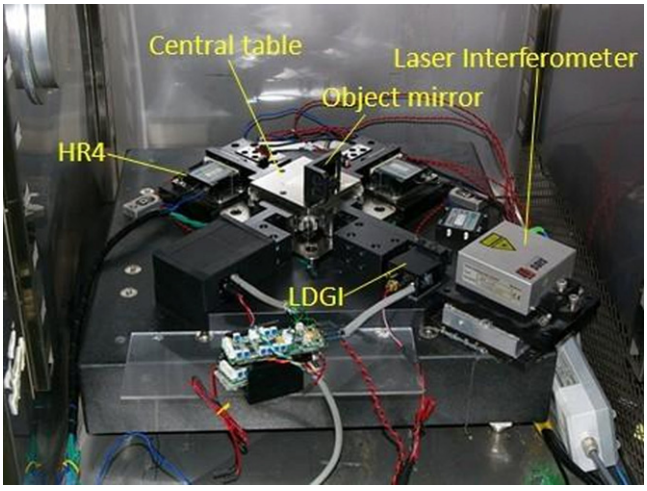

Fig. 14. The experimental setup.

long-stroke nanopositioning control system in association with the new linear stage can achieve the positioning error less than 10 nm and the standard deviation less than 5 nm within the travel range of 15 mm.

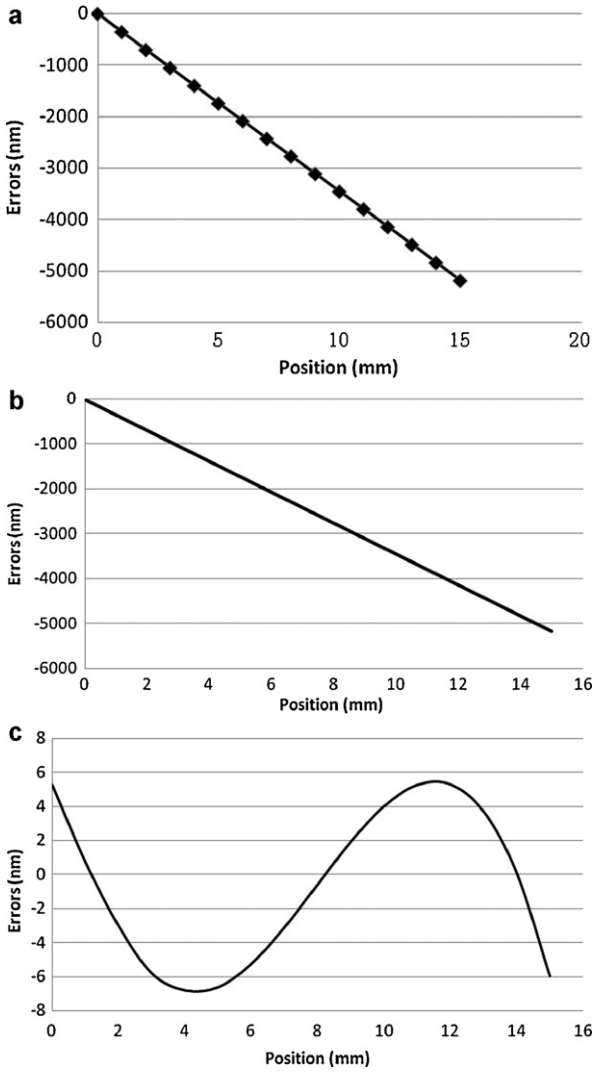

Fig. 15. Positioning error curves.

Table 1
Analysis of positioning errors (unit in nm).

Travel	1st	2nd	3rd	4th	5th	Mean	σ
0.1 mm	0	−5	−3	−1	−5	−2.8	2.3
1 mm	7	2	−1	5	6	3.8	3.3
5 mm	−8	−2	−1	−8	3	−3.2	4.8
10 mm	7	0	−5	−1	6	1.4	5
15 mm	3	−7	0	2	6	0.8	4.9

7. Conclusions

A new long travel linear stage and nanopositioning control system have been presented. Compared with other control systems, the proposed positioning system is featured by some innovative points as below:

1. This system enables a large range-to-resolution ratio and a large accuracy-to-range ratio. With a software-based controller and a hardware-based analog signal processor, a programmable positioning control system has been developed.
2. This control system has good nanopositioning accuracy in various steps up to 15 mm.
3. This control system shows enough stability against some unpredictable disturbance from the environment. The feedback system of LDGI counted by the grating pitch is more stable than the laser interferometer that is counted by the wavelength, which is sensitive to the change of ambient conditions.

Acknowledgements

Parts of this research were sponsored by the National Science Council of Taiwan on the development of a micro-CMM and the National Natural Science Foundation of China under contract number: 50420120134.

References

[1] Shakir H. Multiscale control for nanoprecision positioning systems with large throughput. IEEE Transactions on Control Systems Technology 2007;15:945–51.
[2] Ro PI, Hubbel PI. Nonlinear micro-dynamic behavior of a ball screw driven precision slide system. Precision Engineering 1992;14:229–36.
[3] Steinmetz CR. Sub-micron position measurement and control on precision machine tools with laser interferometer. Precision Engineering 1990;12:12–24.
[4] Takafuji K, Nakashima K. Stiffness of a ball screw with consideration of deformation of the screw, nut and screw thread (preloaded double nut). JSME International Journal Series 3, Vibration, control engineering, engineering for industry 1990;33:620–6.
[5] Zhu Z. Design of a linear piezomotor for positioning feed drives. Ph.D. dissertation, Department of Mechanical Engineering, University of Connecticut; 1995.
[6] Shimizu N, Kimura T, Nakamura T, Umebu I. An ultrahigh vacuum scanning tunneling microscope with a new inchworm mechanism. Journal of Vacuum Science & Technology A 1990;8:333–5.
[7] Chu CL, Fan SH. A novel long-travel piezoelectric-driven linear nanopositioning stage. Precision Engineering 2006;30:85–95.
[8] Okazaki Y, Asano S, Goto T. Dual-servo mechanical stage for continuous positioning. International Journal of the Japan Society for Precision Engineering 1993;27:172–3.
[9] Sakuta A, Ueda K, Ogawa K, Moriwaki Y, Sumiya M. Precision dual positioning system. Proceedings of SPIE 1990;1334:10–7.
[10] Fujita T, Matsubara A, Kono D, Yamaji I. Dynamic characteristics and dual control of a ball screw drive with integrated piezoelectric actuator. Precision Engineering 2010;34:34–42.
[11] Elfizy AT, Bone GM, Elbestawi MA. Design and control of a dual-stage feed drive. International Journal of Machine Tools & Manufacture 2005;45:153–65.
[12] Liu CH, Jywe WY, Jeng YR, Hsu TH, Li YT. Design and control of a long-traveling nano-positioning stage. Precision Engineering 2010;34:497–506.
[13] Kawashima A, Arai T, Tadano K, Fujita T, Kagawa T. Development of coarse/fine dual stage using pneumatically driven bellows actuator and cylinder with air bearings. Precision Engineering 2010;34:526–33.
[14] Liu YT, Li BJ. Precision positioning device using the combined piezo-VCM actuator with friction constraint. Precision Engineering 2010;34:534–45.
[15] Egashira Y, Kosaka K, Endo T, Hashiguchi H, Nagamoto K, Watanabe M, et al. Development of nonresonant ultrasonic motor with sub-nanometer resolution. In: Proceedings of IEEE ultrasonics symposium. 2002. p. 637–40.
[16] Egashira Y, Kosaka K, Takada S, Iwabuchi T, Kosaka T, Baba T, et al. Sub-nanometer resolution ultrasonic motor for 300 mm wafer lithography precision stage. In: Proceedings of IEEE-NANO. 2001. p. 252–3.
[17] Egashira Y, Kosaka K, Iwabuchi T, Kosaka T, Baba T, Endo T, et al. Sub-nanometer resolution ultrasonic motor for 300 mm wafer lithography precision stage. Japanese Journal of Applied Physics 2002;41:5858–63.
[18] Tanaka K, Oka M, Uchibori A, Iwata Y, Morioka H. Precise position control of an ultrasonic motor using the PID controller combined with NN. Electrical Engineering in Japan 2002;122:1317–24.
[19] Zhao X, Chen W, Shi S. Ultrasonic motor's velocity control based on the BP fuzzy neural network with stored information. In: Proceedings of 1st international symposium on systems and control in aerospace and astronautics. 2006. p. 1137–40.
[20] Senjyu T, Miyazato H, Yokoda S, Uezato K. Speed control of ultrasonic motors using neutral network. IEEE Transactions on Power Electronics 1998;13:381–7.
[21] Lin FJ, Wai RJ, Shyu KK, Liu TM. Recurrent fuzzy neural network control for piezoelectric ceramic linear ultrasonic motor drive. IEEE Transactions on Ultrasonic, Ferroelectrics, and Frequency control 2001;48:900–13.
[22] Fan KC, Lai ZF. An intelligent nano-positioning control system driven by an ultrasonic motor. The International Journal of Precision Engineering and Manufacturing 2008;9:40–5.
[23] Fan KC, Cheng F. Nanopositioning control on a commercial linear stage by software error correction. Nanotechnology and Precision Engineering 2006;4(1):1–9.
[24] Fan KC, Fei YT, Yu XF, Chen YJ, Wang WL, Chen F, et al. Development of a low-cost micro-CMM for 3Dmicro/nano measurements. Measurement Science & Technology 2006;17:524–32.
[25] Nanomotion Ltd. AB2 driver user manual. P/N: AB02458000A, www.nanomotion.com; 2003.
[26] Sirisena H, Teng F. Multivariable pole-zero placement self-tuning controller. International Journal of Systems Science 1986;17:345–52.
[27] He SZ, Tan SH, Xu FL, Wang PZ. Fuzzy self-tuning of PID controllers. Fuzzy Sets and Systems 1993;56:37–46.
[28] Hecht-Nielsen R. Neurocomputing. Reading MA: Addison-Wesley Publishing Company; 1990. pp. 124–138.
[29] Psaltis D, Sideris A, Yamamura AA. A multilayered neural network controller. IEEE Control System Magazine 1988;8(2):17–21.
[30] Wang J, Kang LY, Cao BG. Neural network PID control of a distributed power generation system based on renewable energy. Journal of Applied Sciences 2005;5(10):1772–6.
[31] Bryan JB. The Abbé principle revisit: an updated interpretation. Precision Engineering 1979;1:129–32.